IOP Publishing Journal of Physics B: Atomic, Molecular and Optical Physics
J. Phys. B: At. Mol. Opt. Phys. **48** (2015) 214004 (10pp) doi:10.1088/0953-4075/48/21/214004

Coherent control of photoelectron wavepacket angular interferograms

P Hockett[1], M Wollenhaupt[2] and T Baumert[3]

[1] National Research Council of Canada, 100 Sussex Drive, Ottawa, K1A 0R6, Canada
[2] Institut für Physik, Carl von Ossietzky Universität Oldenburg, Carl-von-Ossietzky-Straße 9-11, D-26129 Oldenburg, Germany
[3] Institut für Physik, Universität Kassel, Heinrich-Plett-Str. 40, D-34132 Kassel, Germany

E-mail: paul.hockett@nrc.ca

Received 30 April 2015, revised 4 August 2015
Accepted for publication 19 August 2015
Published 23 September 2015

Abstract

Coherent control over photoelectron wavepackets, via the use of polarization-shaped laser pulses, can be understood as a time and polarization-multiplexed process, where the final (time-integrated) observable coherently samples all instantaneous states of the light–matter interaction. In this work, we investigate this multiplexing via computation of the observable photoelectron angular interferograms resulting from multi-photon atomic ionization with polarization-shaped laser pulses. We consider the polarization sensitivity of both the instantaneous and cumulative continuum wavefunction; the nature of the coherent control over the resultant photoelectron interferogram is thus explored in detail. Based on this understanding, the use of coherent control with polarization-shaped pulses as a methodology for a highly multiplexed coherent quantum metrology is also investigated, and defined in terms of the information content of the observable.

Keywords: coherent control, photoionization, polarization-shaped pulses, photoelectron angular interferograms, information content, metrology

(Some figures may appear in colour only in the online journal)

1. Introduction

In the area of coherent control the coherence properties of light together with quantum-mechanical matter interferences are used to steer a quantum system to a desired target or dynamical behaviour. While original ideas were developed in the physical–chemistry community, the field of quantum control has grown well beyond its traditional boundaries, and a tremendous cross-fertilization to neighboring quantum technologies in terms of both experimental techniques and theoretical developments has occurred [1]. The increasing availability of laser sources operating on the time scale of molecular dynamics, i.e. the femtosecond regime, and the increasing capabilities of shaping light in terms of amplitude, phase and polarization—also on the time scale of molecular dynamics—brought the temporal aspect of this field to the fore (see for example [2] and references therein).

A thoroughly investigated control regime is the case of interferences between N and M photon pathways. As outlined in Shapiro and Brumer [1], there are, in general terms, two types of scenario. In cases where N and M are of the same parity (i.e. both either odd or even), the integral as well as the differential cross section can be controlled as a function of phase between the N photon and M photon field. In cases where N and M have different parity, only the differential cross section, i.e. a scattering process into different angles, can be controlled. In the following we focus specifically on the N = M case. Using two-photon transitions, the transition from 6s → 7d in cesium was studied in two regimes, spanning from optical interferences to quantum interferences, by Girard *et al* [3]. Using pulse shaping technologies, this scheme has been exploited many times. In the perturbative interaction regime the physical process can be related to (higher order) spectral interferences [4–7]. In the non-perturbative interaction regime for one photon transitions control via selective population of dressed states was demonstrated, originally on atoms [8] and, later, used for control of the coupled nuclear and electronic dynamics in molecules [9]. For the one photon perturbative case the transition from optical to quantum interferences was studied on the 4s → 4p transition in

potassium by Girard's group [10] and the same group studied later the coherent buildup of population in Rb ($5s \rightarrow 5p$) during chirped excitation [11]. It turned out that these coherent transients can be used for quantum state measurements [12]. The use of polarization-shaped pulses in multiphoton schemes has been investigated for a range of control and metrology scenarios, including absorption [13], ionization [14, 15], photoemission [16], polarization gating for high harmonic generation [17], multidimension electronic spectroscopy [18] and nano-plasmonics [19].

Such investigations were extended to bound-free transitions, and the interference of free electron wave packets on threshold electrons as well as on the first ATI channel [20] was studied on potassium atoms, a time-domain analogue to Young's double slit experiment. Later these interference investigations were extended to three photon ionization processes with polarization shaped laser pulses [21], tomographic reconstruction techniques were developed to measure the three-dimensional photoelectron momentum distributions [22], and applied to measurements of a $1 + 2$ photon resonantly enhanced ionization process in potassium atoms [23] and to ionization of chiral molecules [24].

Many types of interference can be manifested in continuum photoelectron wavepackets. The simplest case, time-independent photoionization at a single energy, results in an outgoing photoelectron wave with an angular structure defined by the interferences between different angular momentum components (*partial waves*); this phenomenon, and control over the resulting interferograms, has long been investigated in the energy-domain [25–27]. In the time-domain, the possibility of preparing and controlling single or multiple photoelectron wavepackets, allows for the effects of coherence to appear in both the angular and energy structure of the observable photoelectron flux, and thus further possibilities for coherent control methodologies [8, 20, 21]. Regardless of the exact scheme employed, the light–matter interaction involves ionization of a target system, with some form of control over this process via the laser field applied. In the most basic case, control is achieved via the ionization dynamics, in essence by affecting the magnitudes and/or phases of the accessible ionization pathways; in more complex cases the interaction may additionally involve dynamics in the matter system (which may be laser-driven or inherent to the system), and continuum dynamics which occur post-ionization. In the case of ultrafast shaped laser-pulses, the properties of the bound and/or continuum dynamics are interrogated or controlled on the time-scale of the changes in the laser pulse. In this case, there is an inherent coherent temporal multiplexing in the observable photoelectron interferogram: since this observable is integrated over the pulse duration, all polarization states in the shaped laser pulse are sampled. The final observable therefore results from the (cumulative) coherent superposition of *all the ionization pathways which contribute at any instant during the pulse*.

It was recently realized, that these multiplexed data can be used to determine the radial phase shifts of the ionization matrix elements where dynamics in the matter system and in the ionizing pathways were exploited [28]. In this contribution we take the topic of complete ionization studies as an example that coherent control in the time-domain with polarization-shaped pulses represents a powerful tool for metrology. We study the transient build up of the final continuum interference, and argue that—due to the coherent nature of the process—the information on ionization matrix elements can be extracted in a much shorter measurement time as compared to serial ionization schemes with time-independent polarization states. While the determination of ionization matrix elements, which necessitates interrogation of a range of light–matter couplings (*vide infra*), is a natural choice for this polarization-multiplexed metrology, the concept could equally be applied to any coherent, dynamical process controlled and interrogated by shaped laser-pulses, and resulting in a time-integrated observable.

2. Coherent control over photoelectron interferograms

In this theoretical work, we discuss the specific case of coherent control over the angular structure of a photoelectron wavepacket. This concept has been previously demonstrated experimentally, by making use of ultrafast polarization-shaped pulses interacting with, and ultimately ionizing, potassium atoms. This particular scheme incorporates both intra-pulse bound-state dynamics, driven by the moderately intense laser field, and net three-photon ionization. At the one-photon level a near-resonant bound-bound transition, populating 4p states, is strongly driven; this is followed by a much weaker, two-photon ionizing transition of these states. Treating this as a time-dependent one-electron process allows for a schematic description:

$$4s(t) + E(t) \longleftrightarrow 4p_{\pm 1}(t) + E(t) \rightarrow \Psi(\mathbf{k}, t), \qquad (1)$$

where the final continuum wavefunction $\Psi(\mathbf{k}, t)$ is dependent on the photoelectron momentum $\mathbf{k}$ and time t, and $E(t)$ denotes a time-dependent electric field. This scheme is outlined in further detail in [20, 21], and more recently in [28, 29], wherein we focussed primarily on determining the details of the interaction, in particular the determination of the ionization matrix elements from experimental measurements[4]. We focus herein on the coherent control possible with polarization-shaped pulses, making use of the previously determined matrix elements in our calculations, and investigate the time-dependent aspects of the resulting interferograms and their further use for metrology.

We begin with an overview of the details pertinent to the consideration of polarization-shaped pulses. The laser pulse is described generally by the electric field $E(x, y, t)$, i.e. in a Cartesian basis and propagating in the z-direction. This field can be defined in terms of its spectrum $\tilde{E}(\Omega)$ and associated spectral phase ϕ, which we allow to be independent for the

[4] Note that this treatment neglects any intensity-dependence of the ionization dynamics. Experimentally, such effects have not been significant in the 10^{12} and 10^{13} Wcm^{-2} intensity regimes investigated. Intensity-dependent effects, and methods for incorporating such effects, are discussed more generally in [29].

two polarization components:

$$\begin{pmatrix} E_x(t) \\ E_y(t) \end{pmatrix} = \mathcal{F}^{-1}\left\{ \tilde{E}(\Omega) \begin{pmatrix} e^{i\phi_x(\Omega)} \\ e^{i\phi_y(\Omega)} \end{pmatrix} \right\}. \quad (2)$$

In this form, shaping of the polarization of the field is defined by the spectral phases $\phi_x(\Omega)$ and $\phi_y(\Omega)$. A field with $\phi_x = \phi_y$ over the full spectrum will be linearly polarized; a field with a frequency-independent phase shift ($\phi_x \neq \phi_y$) will be in a 'pure' elliptical or circular state, with no time-dependence of the polarization; a field with a frequency-*dependent* phase shift will produce a fully polarization-shaped pulse, with a complex temporal-dependence of the polarization and spectral content of the pulse [30]. For the shaped pulses explored in this manuscript, the spectral phase is set to a single value for the red-half of the pulse and y-component only, and is zero elsewhere, i.e. there is a phase step defined as:

$$\phi_y(\Omega) = \begin{cases} \phi_y, & \Omega < \Omega_0, \\ 0, & \Omega \geqslant \Omega_0, \end{cases} \quad (3)$$

$$\phi_x(\Omega) = 0, \quad (4)$$

where Ω_0 is the central frequency of the pulse. Within this definition, the full spectral phase function $\phi_y(\Omega)$ is parametrized by the single value ϕ_y, and this value is used to label the shaped pulses in this work. (For more general discussion of pulse-shapes arising from spectral phase steps, the reader is referred to [31].)

For the case of a polarization-shaped pulse, it is convenient to express the pulse in terms of left and right circularly polarized components, $E_L(t)$ and $E_R(t)$. For atomic ionization this is also a good choice of basis, since the left and right circularly polarized components will couple to different m-states, specifically to $-m$ and $+m$ states respectively [28].

$$\begin{pmatrix} E_L(t) \\ E_R(t) \end{pmatrix} = \frac{1}{\sqrt{2}} \begin{pmatrix} E_x(t) - iE_y(t) \\ E_x(t) + iE_y(t) \end{pmatrix}. \quad (5)$$

In this basis we can also express the helicity of the pulse, which we define as the normalized difference between the $E_L(t)$ and $E_R(t)$ components:

$$H(t) = \frac{|E_R(t)| - |E_L(t)|}{|E_R(t)| + |E_L(t)|}. \quad (6)$$

Hence, $H(t) = 1$ for a field which is right circularly polarized at time t, $H(t) = -1$ for a left circularly polarized field, and $H(t) = 0$ for a linearly polarized field. All other values define varying degrees of ellipticity, with an overall right or left handedness for positive or negative helicities respectively. The behaviour of $H(t)$ is thus equivalent to the (normalized) $S_3(t)$ Stokes parameter, which also parametrizes the degree of R or L polarization and takes values on the interval $+1 \geqslant S_3 \geqslant -1$ [32], but is defined directly from the L/R electric field basis.

Examples of the pulse shapes arising from spectral phase steps, as defined by equation (3), are given in figure 1. In all cases the pulse is initially defined to be Gaussian, with bandwidth matching the transform-limited pulse duration of $\tau = 60$ fs (full-width, half max), and is linearly polarized. The application of a phase-step, with value ϕ_y, results in a temporally varying polarization state as discussed above, with the pulse passing through various degrees of ellipticity as a function of the magnitudes and phases of the $E_L(t)$ and $E_R(t)$ components. The colour-map in figure 1 shows this time-dependence in terms of the helicity $H(t)$ (equation (6)), which is most directly related to the contributing ionization pathways

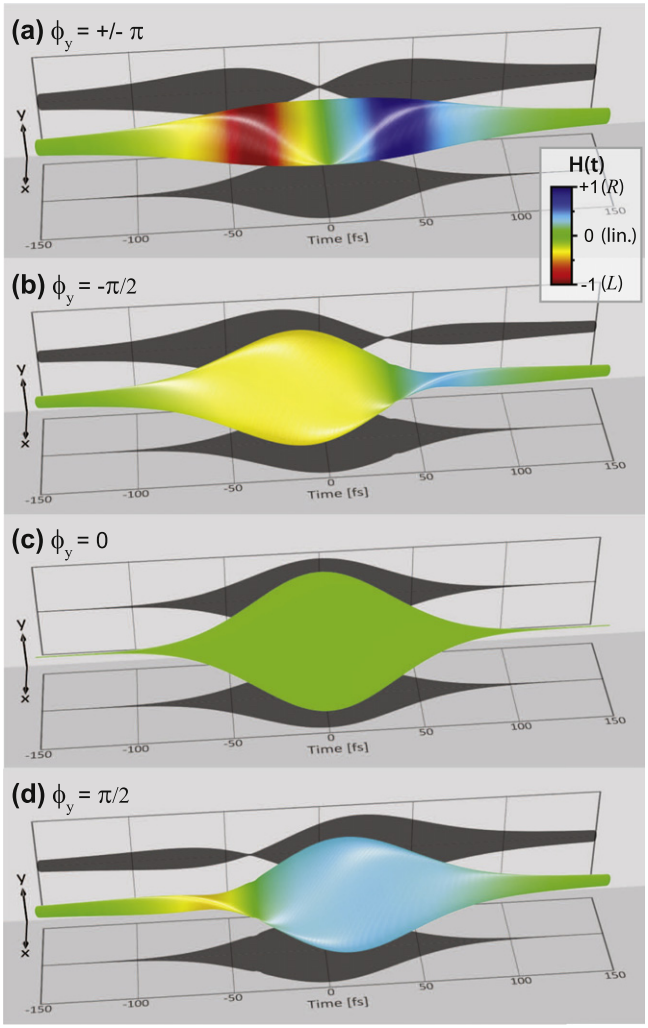

Figure 1. Polarization-shaped pulses $E(x, y, t)$, resulting from a phase step applied to the spectral phase, as defined by equation (3). The helicity, $H(t)$ (equation (6)), is shown by the colour-map. The photoelectron interferograms resulting from these pulses are shown in figure 2.

For the net three-photon ionization of potassium, outlined above (equation (1)), which we use here as our exemplar system, the overall process to a final state f can be written as:

$$d_f(\mathbf{k}, t) = \sum_{i,v} d_{i\to v}(\mathbf{k}, t) d_{v\to f}(\mathbf{k}, t) \chi_i(t), \quad (7)$$

where $d_f(\mathbf{k}, t)$ is the effective two-photon ionization dipole moment, defined as a product of two one-photon terms (from

an initial state i to a final state f via a virtual state v) and the ionizable $4p_{\pm1}$ state population $\chi_i(t)$.

The final observable photoelectron interferogram is given by the coherent square over all final continuum states, and can be written as:

$$I(\theta, \phi; k) = \iint \mathrm{d}k\ \mathrm{d}t \sum_{f,f'} d_f(\mathbf{k}, t) d^*_{f'}(\mathbf{k}, t), \tag{8}$$

$$= \iint \mathrm{d}k\ \mathrm{d}t \sum_{\substack{l,m \\ l',m'}} d_{l,m}(k, t) Y_{l,m}(\theta, \phi) d^*_{l',m'}(k, t) Y^*_{l',m'}(\theta, \phi), \tag{9}$$

$$\equiv \iint \mathrm{d}k\ \mathrm{d}t \sum_{\substack{l,m \\ l',m'}} \psi_{l,m}(\mathbf{k}, t) \psi^*_{l',m'}(\mathbf{k}, t). \tag{10}$$

Here the final continuum states are expressed in terms of angular momentum states (l, m), with spatial angular dependence given by spherical harmonics $Y_{l,m}(\theta, \phi)$. Equivalently, the expression can be given in terms of the components of the continuum photoelectron wavefunction $\Psi(\mathbf{k}, t) = \sum_{l,m} \psi_{l,m}(\mathbf{k}, t)$, which most clearly define the origin of the observable photoelectron interferogram. The final energy and angle-resolved observable is the coherent square of this continuum wavefunction, integrated over time t and photoelectron energy k, for a small energy range dk over which we assume the ionization dipole moments $d_{l,m}(k, t)$ are constant. As discussed above, it is the coherent nature of the temporal integration which provides the multiplexing inherent to the final interferogram. Spcifically, for polarization-shaped pulses, integration of the final observable over the laser pulse envelope (i.e. $t > \tau$) provides a polarization-multiplexed measurement over all (instantaneous) polarization states sampled by the pulse.

In terms of control, the details of the laser field affect both the bound-state populations $\chi_i(t)$, and their coupling to the final continuum states $\psi_{l,m}(\mathbf{k}, t)$. The details of the bound-continuum coupling have been previously determined (see [28, 29] for further details), therefore the effect of the polarization-shaped laser field can be investigated numerically, via computation of the time-dependent excited state populations $\chi_i(t)$ for any given laser pulse, and application of equations (7) and (8). In the following section we explore this coherent control methodology in terms of the intra-pulse dynamics, and further considerations for applications to coherent metrology are discussed in the final section.

3. Photoelectron interferograms from shaped pulses

To illustrate the control of continuum wavepackets with polarization-shaped pulses, figure 2 shows examples for four different pulse shapes. Here the pulse shapes are parametrized as defined in equation (3), by the spectral phase ϕ_y which is applied to the red half of the pulse spectrum for the $E_y(t)$ component only. For $\phi_y = 0$ the pulse is unchanged from its initial linear polarization state, and a cylindrically symmetric distribution is observed (figure 2(c)), while for all other cases the resultant continuum wavefunction is more complicated, and reflects both the laser-driven bound-state dynamics and ionization dynamics, integrated coherently over the pulse duration.

To illustrate these dynamics, inherent to the control process, figure 3 shows the temporal behaviour of the continuum wavefunction. In this example, $\phi_y = -\pi$; the resulting pulse shape was already shown in terms of the spatio-temporal function $E(x, y, t)$ in figure 1(a), and is shown in terms of the $E_{\mathrm{L/R}}$ components in figure 3(a). This pulse has a double-peaked structure in terms of the $E_{\mathrm{L/R}}$ components of the field, hence a pulse which is close to pure circular polarization states in temporal regions where one component dominates, and passes through varying degrees of ellipticity as the $E_{\mathrm{L}} : E_{\mathrm{R}}$ ratio changes. This is shown most directly by the helicity $H(t)$ (equation (6)), shown by the dashed line in panel (a). Figure 3(b) shows the amplitudes of the instantaneous contributions to the continuum wavefunction, $\psi_{l,m}(t)$. These amplitudes follow closely the $E_{\mathrm{L}}(t)$ and $E_{\mathrm{R}}(t)$ field components since, as mentioned above, these components drive the ionization towards $m < 0$ and $m > 0$ states respectively. At any given instant t, the photoelectron interferogram is given by the coherent square of the continuum wavefunction, hence will depend on the amplitudes and phases of the $\psi_{l,m}(t)$ components, and a few examples are shown in figure 3(d). Similarly, figures 3(c) and (e) show the cumulative continuum wavefunction, i.e. the coherent temporal sum over $\psi_{l,m}(t)$ up to time t, and resultant photoelectron interferograms. These plots therefore indicate the coherent evolution of the final angular interferogram; as continuum population builds-up over the laser pulse, the instantaneous and cumulative interferograms diverge. These results highlight the sensitivity of the final state wavefunction, and resultant interferogram, to the exact shape of the pulse, and the inherent polarization-multiplexing.

In this example, the double-peaked nature of the pulse in the $E_{\mathrm{L/R}}$ basis is particularly apt for consideration of the coherent build-up of the continuum wavefunction. The instantaneous contribution to the continuum for pure left and pure right circularly polarized light are identical, aside from the sign of the m terms prepared, which only affects the handedness of the phase of $\psi_{l,m}$ with respect to the angle ϕ. Therefore, in ionization with a pure circular polarization state, only final states with $l = 3$ and $m = +3$ or $m = -3$ would be populated, and a ϕ-invariant interferogram would result. However, if both states are populated and interfere, the ϕ-invariance is broken due to the opposite phase of the states, which is given by $\mathrm{e}^{-im\phi}$. This is the essence of polarization-multiplexing, in which continuum contributions correlated with ionization from different polarization states can interfere. With a polarization-shaped pulse, this interference occurs temporally, with the coherent build-up of the continuum wavefunction over the pulse. In the case illustrated here, the complexity is increased somewhat and there is significant population of $m = \pm1$ (for both $l = 1$ and $l = 3$) states over parts of the pulse, resulting in an observable with rich angular structure (handedness and/or multiple lobes) for many of the instantaneous contributions, as well as in the cumulative

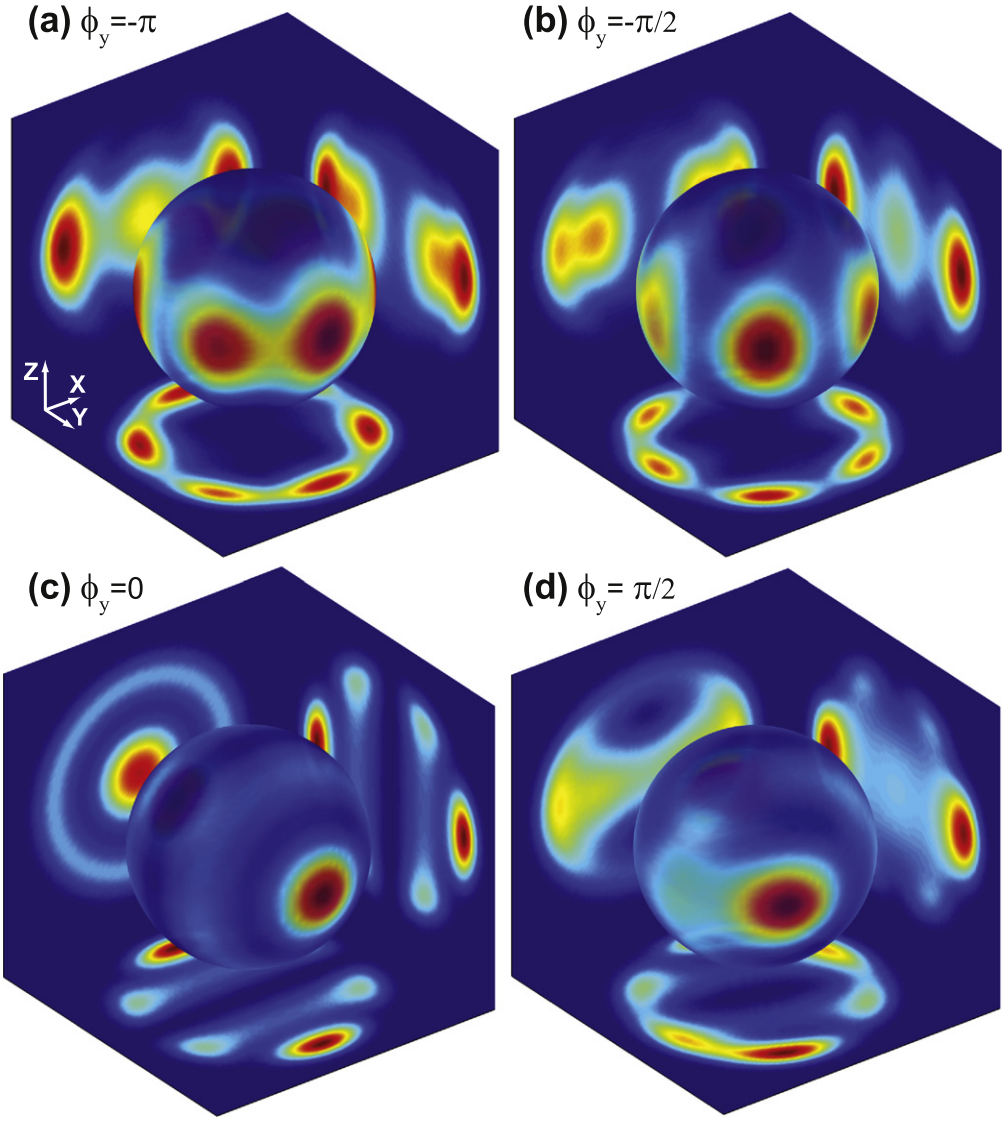

Figure 2. Photoelectron interferograms from polarization-shaped laser pulses. The angular interferograms $I(\theta, \phi; k)$ are shown on an isosphere corresponding to a single k, and 2D projection planes of the interferograms are also shown (here a Gaussian radial distribution $G(k)$ is assumed, see [29] for numerical details). The axis convention is shown in panel (a), and the z-axis defines the laser propagation direction; the corresponding shaped laser pulses, $E(x, y, t)$, parametrized by a spectral phase ϕ_y, are shown in figure 1.

interferogram; despite this complexity the underlying mechanism of temporal polarization-multiplexing is conceptually identical to the simpler case described above. This process is also functionally identical to the time-domain interferences observed in the photoelectron energy spectrum following ionization by a double-pulse, as discussed in [20]. In that case the polarization of both pulses was linear, but the addition of a temporal phase to the electron wavepackets, via the use of two time-separated pulses, created additional interferences which could be observed in the (time-integrated) photoelectron energy spectrum as a function of the temporal phase. In all cases, the final observable maintains coherence over the photoelectron wavepacket(s), allowing for coherent control over this observable via the applied electric field(s). Conceptually, all of these cases with doublet-structured pulses are time-domain analogues of Young's double slit, in which phase control is applied in the temporal rather than spatial dimension [22, 33], although the simple analogy belies the rapid increase in complexity (beyond simple doublet structures) which can be readily achieved in the time-domain.

4. Coherent control for metrology

In the preceding section we focussed on the sensitivity of the final continuum wavefunction to polarization-shaped pulses, in the case where the details of the bound-continuum coupling are known. The opposite also holds: this sensitivity can be used as a coherent quantum metrology in order to discern details of the ionization dynamics. In fact, it was this sensitivity that enabled the bound-continuum couplings to be determined (see [28, 29]), although polarization-shaped pulses were not exploited in that case. A natural question which arises in this context is whether pulse-shapes can be tailor-

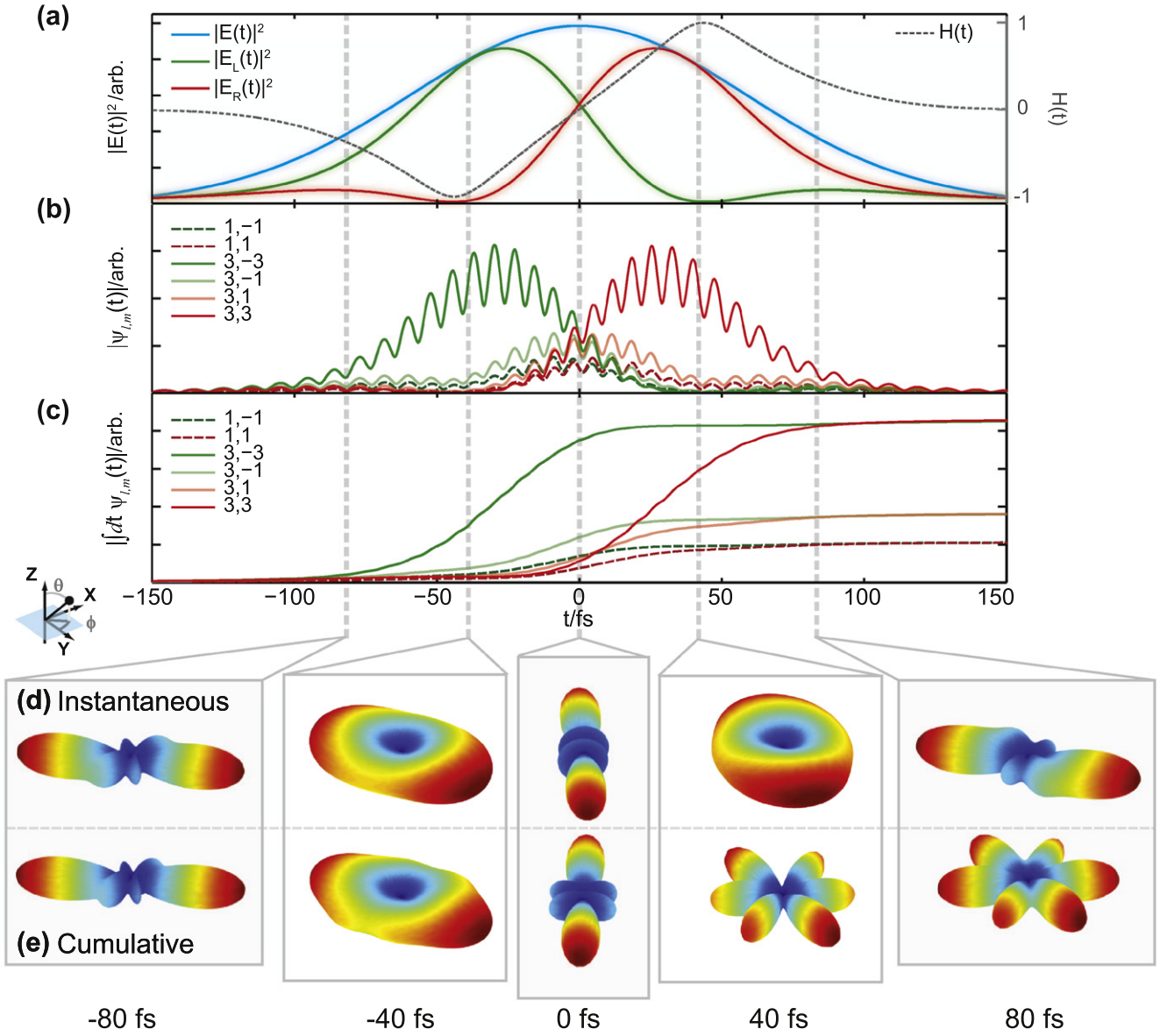

Figure 3. Intrapulse continuum dynamics. (a) Shaped laser pulse for a spectral phase step $\phi_y = -\pi$, expressed in the L/R basis, and helicity $H(t)$. This is the same pulse as shown in figure 1(a). (b) Instantaneous contribution to the continuum wavefunction Ψ, for each partial-wave channel $\psi_{l,m}$. (c) Cumulative continuum wavefunction $\int \mathrm{d}t\psi_{l,m}(t)$. (d) Instantaneous and (e) cumulative photoelectron interferograms, $\Psi^*\Psi$, plotted in polar form. The final cumulative result corresponds to the interferogram shown in figure 2(a).

made for a particular measurement, and what benefit this carries over a set of serial measurements with no polarization-multiplexing. Although this possibility has been discussed in previous work in general terms, the details have yet to be explored.

To approach this question, one must first consider the nature of the metrology, and the information content required from an observable. In this case we are concerned with 'complete' photoionization experiments, in which the bound-continuum couplings—the magnitudes and phases of the ionization matrix elements—are determined [34]. Clearly, this information is available from the photoelectron interferograms, since they are the coherent sum over all contributing continuum channels $\psi_{l,m}$, hence sensitive to both the amplitudes and phases of these channels. However, for any single polarization state, the interferences present will be limited by the bound-continuum couplings inherent to the light–matter system, so a single measurement will not usually contain enough information to uniquely determine the full set of $\psi_{l,m}$ present. Therefore, in a serial measurement scheme, a set of interferograms are obtained by varying the laser polarization (or via other means of altering only the geometric aspects of the problem, see [28, 29, 34] and references therein for further discussion) are obtained, and analysed globally to obtain the underlying properties. A polarization-multiplexed measurement therefore represents a powerful alternative, since all possible ionization channels may be accessed coherently, as a function of time, over the pulse duration. This allows for the possibility of rapid photoelectron metrology in general, and also for high-sensitivity measurements by the

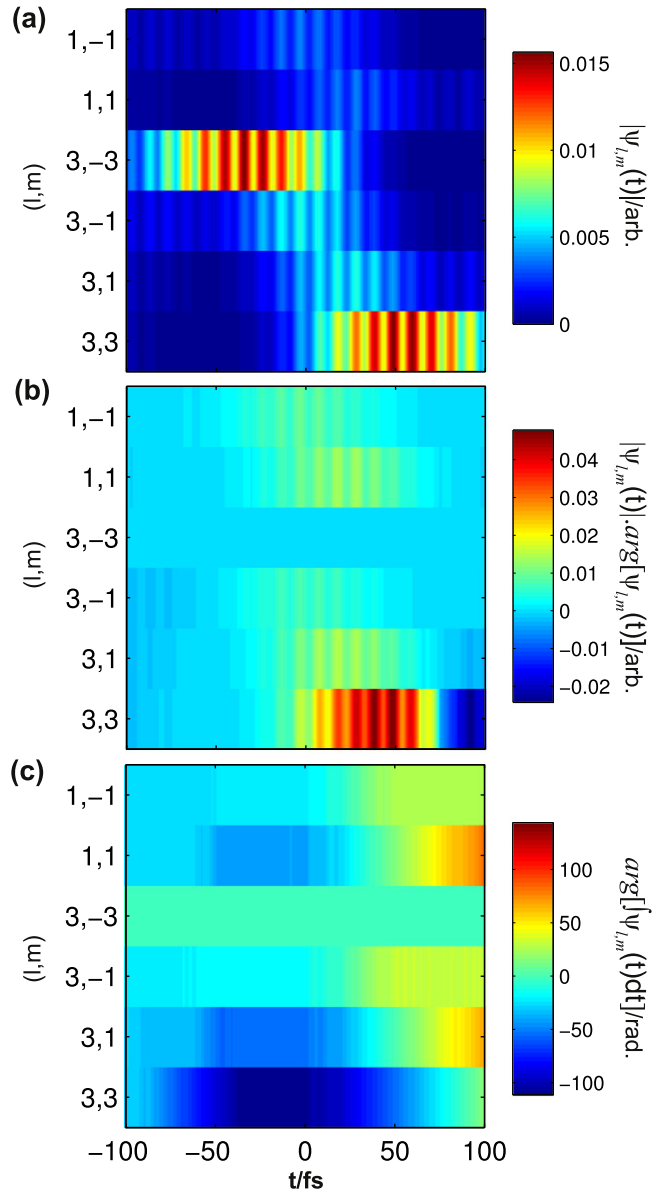

Figure 4. Interferences in the continuum wavefunction. (a) magnitude of the continuum wavefunction components $\psi_{l,m}(t)$, shown for all contributing (l, m) components; (b) instantaneous phase contributions, $\arg[\psi_{l,m}(t)]$, relative to the reference phase $\arg[\psi_{3,-3}(t)]$ and weighted by the magnitude of the channel; (c) cumulative continuum phase $\arg[\int dt\psi_{l,m}(t)]$, relative to the reference phase $\arg[\int dt\psi_{3,-3}(t)]$. These results are for a shaped pulse with $\phi_y = -\pi$, as shown in figure 1(a).

choice of pulse-shapes which target certain channels or interferences. With respect to coherent control of chemical reactions, this analysis underscores the findings that complex shaped laser pulses can be more selective as compared to simple pulse shapes [35, 36], and is confluent with suggestions to use specifically shaped light fields for a spectroscopy ansatz going beyond the typical pulse sequence spectroscopy with Fourier limited pulses [2, 37].

To highlight the potential of this coherent control scheme for metrology, figure 4 illustrates the relative amplitude and phase contributions, as a function of time, for the same $\phi_y = -\pi$ case discussed in the previous section. In these results, the phases are referenced to the $\psi_{3,\ -3}(t)$ channel, and shown for both instantaneous contributions to the continuum wavepacket $\psi_{l,\ m}(t)$, and cumulative continuum components $\int dt\psi_{l,m}(t)$. In the instantaneous case, figure 4(b), the results are weighted by the amplitudes of the channels to better visualize the interferences present at any given t, while the cumulative phase is shown without such weighting. This figure presents a more comprehensive, but less intuitive, time-domain picture of the creation of the continuum wavepacket than the discrete angular-interferograms of figures 3(d) and (e), since it indicates the contributing interferences for all time-steps. As discussed generally above, and in the previous section, these results indicate how the various continuum channels build up coherently over the laser pulse. Although the specific details are complicated, it is clear that the instantaneous contributions sample many different interferences—different relative magnitudes and phases between the set of contributing (l, m) channels—which coherently add over the temporal coordinate to produce the final observable.

More explicitly, these results can be considered in terms of the information content of the observable. In the case of measurements based on pulse polarization, all possible measurements exist in the space of all possible pulse polarizations, $\{H\}$. A time-invariant helicity, denoted $\bar{H}(\bar{\phi}_y)$, corresponds to a single point in this measurement space, parametrized by the spectrally invariant phase $\bar{\phi}_y$, while a time-dependent helicity $H(t;\ \phi_y(\Omega))$, parametrized by a spectral phase function $\phi_y(\Omega)$, samples a sub-set of points within this space. Figure 5 illustrates this sampling of the pulse polarization space, expressed in terms of time-dependent Stokes parameters $S_n(t)$ (normalized by $S_0(t)$) and plotted on a Poincaré sphere. Here the paths on the sphere show the time-dependent sampling by a polarization-shaped pulse created by a spectral phase-step of the type defined in equation (3), for the pulses shown in figure 1. For the case of $\phi_y = 0$ there is no time-dependence to the pulse polarization, hence only a single point in the polarization space is sampled, while for all other ϕ_y a range of polarization states are sampled.

To quantify the information content of a measurement, we can therefore consider the size of the measurement space sampled by a single measurement, or set of measurements. The information content of a single measurement with a single polarization state is given as $M(\bar{H}(\bar{\phi}_y))$, and a set of serial measurements therefore has an information content of $M_s = \sum_{\bar{\phi}_y} |M(\bar{H}(\bar{\phi}_y))|$, where the modulus is used to emphasize the fact that each measurement is incoherent with respect to all others. Similarly, a single polarization-multiplexed measurement has an information content given by $M_p = |\int dt\ M(H(t;\ \phi_y(\Omega)))|$, and the modulus is used to emphasize the coherent nature of the parallel case. A set of parallel measurements has information content $(M_p)_s = \sum_{\phi_y(\Omega)} M_p = \sum_{\phi_y(\Omega)} |\int dt\ M(H(t;\ \phi_y(\Omega)))|$, where each independent measurement corresponds to a laser pulse

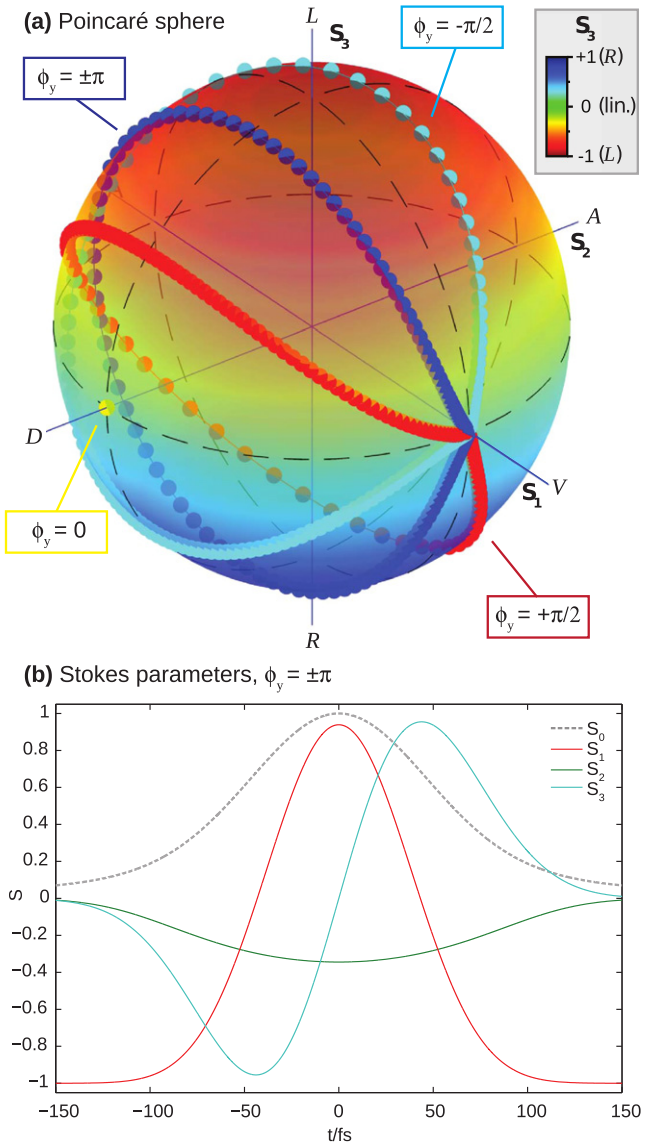

Figure 5. Sampling paths in polarization space, defined by the time-dependent Stokes parameters (S_1, S_2, S_3) and plotted on a Poincaré sphere. (a) Poincaré sphere. Each path on the sphere corresponds to a polarization-shaped pulse created by a spectral phase-step of the type defined in equation (3), as shown in figure 1, with points plotted every 2.5 fs. The paths are parametrized by the Stokes parameters, corresponding to the polarization basis states (H, V), (D, A) and (L, R) respectively [32]. The surface colour-map additionally indicates the S_3 value, hence the pulse polarization in the L/R basis. (b) Time-dependence of the Stokes parameters $S_n(t)$ (here normalized by division by $S_0(t)$) for the pulse defined by $\phi_y = \pm\pi$.

defined by a spectral phase function $\phi_y(\Omega)$, and is incoherent with respect to all other pulses.

For an incoherent process, the information content of M_s and M_p are equivalent for the case where $H(t;\, \phi_y(\Omega)) = \sum_{\bar{\phi}_y} \bar{H}(\bar{\phi}_y)$, i.e. the time-dependent pulse samples the same set of points in the measurement space as sampled by the set of measurements M_s. Conceptually, this would correspond to the case where the instantaneous photoelectron interferograms (figure 3(d)) are summed incoherently, hence a set of serial measurements of these interferograms would be identical to the result obtained with the shaped-pulse. In this case, we can define an advantage in terms of the scaling of the measurement time with the size of the polarization sub-space: there is an advantage to a parallel measurement of $(N(\bar{\phi}_y) - 1)T$, where $N(\bar{\phi}_y)$ is the number of measurements sampled, and T the time required per measurement, assumed to be the same regardless of the complexity of the pulse structure.

However, for a coherent process, the information content of the final result for the shaped-pulse case benefits from the fact that the coherent addition over the measurement sub-space is massively parallel, with many additional interferences accessed—this is truly a multiplexing advantage, conceptually equivalent to the massive parallelization inherent to quantum computing. Figure 4 visualizes this multiplexed process, since each temporal slice represents a specific point within the H-space (i.e. one point on the sampling path shown in figure 5(a)). Figure 4(b), which shows the time-dependent contributions to the interferogram for each continuum channel, relative to the reference channel, indicates the specifics of each point in the sampled H-space for any given channel (similarly, figure 3(d) shows the resulting angular-interferograms for a few of these points). Here, both positive and negative contributions are observed relative to the reference, indicating the sampling of points in H-space with different relative phases. Figure 4(c) shows the cumulative effect for the coherent temporal addition of these H-space points on the relative phase of each channel, again showing how the various channels can pass through regions in H-space with constructive or destructive interferences as the continuum wavepacket builds up, hence each point sampled can affect the final interferogram distinctly.

In fact, in this particular case, many of these interferences could not be accessed by serial measurement schemes since, by definition, they cannot sample interferences between different points in H-space (i.e. different points on the Poincaré sphere of figure 5). In order to sample such points, a serial measurement scheme based on interfering the photoelectron wavepackets produced by two pulses of different helicity would be required, such that the information content would be defined by the sum over pairs of helicities: $M_{s*} = \sum_{\bar{\phi}_y, \bar{\phi}_y} |M(\bar{H}(\bar{\phi}_y))M(\bar{H}(\bar{\phi}_y'))|$. In this case, the scaling law for measurement time reflects the square of the sub-space sampled, $N(\bar{\phi}_y)N(\bar{\phi}_y')T = N(\bar{\phi}_y)^2 T$. However, since the parallel case maintains coherence over all measurement points, a single measurement with a shaped-pulse which samples the same sub-space, i.e. $H(t;\, \phi_y(\Omega)) = \sum_{\bar{\phi}_y} \bar{H}(\bar{\phi}_y)$ as defined above, has the same information content, and is obtained in a measurement time T. Here the measurement time saving will scale on $\mathcal{O}(N^2)$, with value $(N(\bar{\phi}_y)^2 - 1)T$. Hence, coherent control in the time-domain represents a powerful tool for metrology, with a high information content measurement obtainable in a short measurement time, as compared to serial measurement schemes.

5. Conclusions

Photoelectron angular interferograms are a high information-content observable. Coherent control over continuum photoelectron wavepackets via the use of polarization-shaped laser pulses translates to a high degree of control over this observable, while a deep understanding of this observable provides a means to a coherent quantum metrology for photoionization processes, including dynamics, with an inherent multiplexing advantage.

Here we have explored these points by analysing, in detail, the computational results and specific details of a single polarization-shaped pulse, and used this to highlight the general concepts. The information content of such measurements was investigated, in contrast to measurements with pulses of a single polarization state, and seen to provide a significant multiplexing advantage in terms of the inherent information content of the measurement, and the measurement time required to obtain the same information content via a set of serial measurements.

Acknowledgments

We thank R Lausten for helpful discussion. Financial support by the State Initiative for the Development of Scientific and Economic Excellence (LOEWE) in the LOEWE-Focus ELCH is gratefully acknowledged.

References

[1] Shapiro M and Brumer P 2011 *Quantum Control of Molecular Processes* (Weinheim, Germany: Wiley-VCH Verlag GmbH and Co. KGaA)
[2] Wollenhaupt M and Baumert T 2011 Ultrafast laser control of electron dynamics in atoms, molecules and solids *Faraday Discuss.* **153** 9
[3] Blanchet V, Nicole C, Bouchene M-A and Girard B 1997 Temporal coherent control in two-photon transitions: from optical interferences to quantum interferences *Phys. Rev. Lett.* **78** 2716–9
[4] Meshulach D and Silberberg Y 1998 Coherent quantum control of two-photon transitions by a femtosecond laser pulse *Nature* **396** 239–42
[5] Präkelt A, Wollenhaupt M, Sarpe-Tudoran C and Baumert T 2004 Phase control of a two-photon transition with shaped femtosecond laser-pulse sequences *Phys. Rev.* A **70** 1–10
[6] Walowicz K A, Pastirk I, Lozovoy V V and Dantus M 2002 Multiphoton intrapulse interference: I. Control of multiphoton processes in condensed phases *J. Phys. Chem.* A **106** 9369–73
[7] Ruge M, Wilcken R, Wollenhaupt M, Horn A and Baumert T 2013 Coherent control of colloidal semiconductor nanocrystals *J. Phys. Chem.* C **117** 11780–90
[8] Wollenhaupt M, Assion A, Bazhan O, Horn Ch, Liese D, Sarpe-Tudoran Ch, Winter M and Baumert T 2003 Control of interferences in an Autler–Townes doublet: symmetry of control parameters *Phys. Rev.* A **68** 15401
[9] Bayer T, Braun H, Sarpe C, Siemering R, Von Den Hoff P, De Vivie-Riedle R, Baumert T and Wollenhaupt M 2013 Charge oscillation controlled molecular excitation *Phys. Rev. Lett.* **110** 1–5
[10] Bouchene M A, Blanchet V, Nicole C, Melikechi N, Girard B, Ruppe H, Rutz S, Schreiber E and Wöste L 1998 Temporal coherent control induced by wave packet interferences in one and two photon atomic transitions *Eur. Phys. J. D*
[11] Zamith S, Degert J, Stock S, de Beauvoir B, Blanchet V, Bouchene M A and Girard B 2001 Observation of coherent transients in ultrashort chirped excitation of an undamped two-level system *Phys. Rev. Lett.* **87** 033001
[12] Monmayrant A, Chatel B and Girard B 2006 Quantum state measurement using coherent transients *Phys. Rev. Lett.* **96** 2–5
[13] Dudovich N, Oron D and Silberberg Y 2004 Quantum control of the angular momentum distribution in multiphoton absorption processes *Phys. Rev. Lett.* **92** 103003
[14] Brixner T, Krampert G, Pfeifer T, Selle R, Gerber G, Wollenhaupt M, Graefe O, Horn C, Liese D and Baumert T 2004 Quantum control by ultrafast polarization shaping *Phys. Rev. Lett.* **92** 208301
[15] Suzuki T, Minemoto S, Kanai T and Sakai H 2004 Optimal control of multiphoton ionization processes in aligned I 2 molecules with time-dependent polarization pulses *Phys. Rev. Lett.* **92** 133005
[16] Golan B, Fradkin Z, Kopnov G, Oron D and Naaman R 2009 Controlling two-photon photoemission using polarization pulse shaping *J. Chem. Phys.* **130** 0–6
[17] Oron D, Silberberg Y, Dudovich N and Villeneuve D M 2005 Efficient polarization gating of high-order harmonic generation by polarization-shaped ultrashort pulses *Phys. Rev.* A **72** 2–5
[18] Voronine D V, Abramavicius D and Mukamel S 2007 Manipulating multidimensional electronic spectra of excitons by polarization pulse shaping *J. Chem. Phys.* **126** 044508
[19] Aeschlimann M, Bauer M, Bayer D, Brixner T, Javier García de Abajo F, Pfeiffer W, Rohmer M, Spindler C and Steeb F 2007 Adaptive subwavelength control of nano-optical fields *Nature* **446** 301–4
[20] Wollenhaupt M *et al* 2002 Interferences of ultrashort free electron wave packets *Phys. Rev. Lett.* **89** 173001
[21] Wollenhaupt M, Krug M, Köhler J, Bayer T, Sarpe-Tudoran C and Baumert T 2009 Photoelectron angular distributions from strong-field coherent electronic excitation *Appl. Phys.* B **95** 245–59
[22] Wollenhaupt M, Lux C, Krug M and Baumert T 2013 Tomographic reconstruction of designer free-electron wave packets *Chemphyschem: Chem Phys Chem* **14** 1341–9
[23] Wollenhaupt M, Krug M, Köhler J, Bayer T, Sarpe-Tudoran C and Baumert T 2009 Three-dimensional tomographic reconstruction of ultrashort free electron wave packets *Appl. Phys.* B **95** 647–51
[24] Lux C, Wollenhaupt M, Sarpe C and Baumert T 2015 Photoelectron circular dichroism of bicyclic ketones from multiphoton ionization with femtosecond laser pulses *ChemPhysChem* **16** 115–37
[25] Cooper J and Zare R N 1968 Angular distribution of photoelectrons *J. Chem. Phys.* **48** 942
[26] Yin Y-Y, Chen C, Elliott D and Smith A 1992 Asymmetric photoelectron angular distributions from interfering photoionization processes *Phys. Rev. Lett.* **69** 2353–6
[27] Yin Y-Y, Elliott D S, Shehadeh R and Grant E R 1995 Two-pathway coherent control of photoelectron angular distributions in molecular NO *Chem. Phys. Lett.* **241** 591–6
[28] Hockett P, Wollenhaupt M, Lux C and Baumert T 2014 Complete photoionization experiments via ultrafast coherent control with polarization multiplexing *Phys. Rev. Lett.* **112** 223001

[29] Hockett P, Wollenhaupt M, Lux C and Baumert T 2015 Complete photoionization experiments via ultrafast coherent control with polarization multiplexing: II. Numerics and analysis methodologies *Phys. Rev.* A **92** 013411
[30] Brixner T and Gerber G 2001 Femtosecond polarization pulse shaping *Opt. Lett.* **26** 557–9
[31] Wollenhaupt M, Bayer T, Vitanov N V and Baumert T 2010 Three-state selective population of dressed states via generalized spectral phase-step modulation *Phys. Rev.* A **81** 1–9
[32] Guenther R 1990 *Modern Optics* (New York: Wiley)
[33] Wollenhaupt M, Bayer T and Baumert T 2014 Control of ultrafast electron dynamics with shaped femtosecond laser pulses: from atoms to solids *From Atoms and Molecules to Clusters, Nanostructures and Solids. Recent Research Topics using Novel Light Sources* ed S Gräfe and M Kitzler-Zeiler (Berlin: Springer) in press
[34] Reid K L 2003 Photoelectron angular distributions *Annu. Rev. Phys. Chem.* **54** 397–424
[35] Assion A, Baumert T, Bergt M and Brixner T 1998 Control of chemical reactions by feedback-optimized phase-shaped femtosecond laser pulses *Science* **282** 919–22
[36] Brixner T, Damrauer N H, Niklaus P and Gerber G 2001 Photoselective adaptive femtosecond quantum control in the liquid phase *Nature* **414** 57–60
[37] Wohlleben W, Buckup T, Herek J L and Motzkus M 2005 Coherent control for spectroscopy and manipulation of biological dynamics *ChemPhysChem* **6** 850–7